IEEE Photonics Journal
An IEEE Photonics Society Publication

Near-Field Transmission-Type Microwave Imaging for Noninvasive Evaluation of Electromagnetic Characteristics: Toward Early Breast Tumor Detection

Volume 9, Number 6, Deccember 2017

Shanwen Luo
Zhong Ji
Sihua Yang
Da Xing

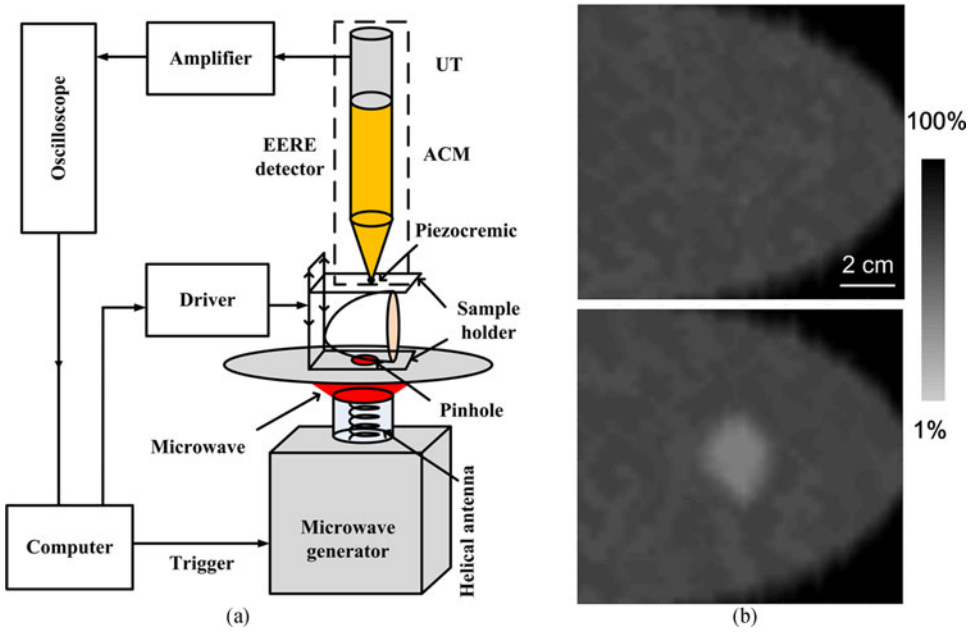

DOI: 10.1109/JPHOT.2017.2765358
1943-0655 © 2017 IEEE

Near-Field Transmission-Type Microwave Imaging for Noninvasive Evaluation of Electromagnetic Characteristics: Toward Early Breast Tumor Detection

Shanwen Luo, Zhong Ji, Sihua Yang, and Da Xing

MOE Key Laboratory of Laser Life Science, Institute of Laser Life Science, South China Normal University, Guangzhou 510631, China

DOI:10.1109/JPHOT.2017.2765358

Manuscript received September 5, 2017; accepted October 18, 2017. Date of publication October 24, 2017; date of current version November 6, 2017. This work was supported in part by the National Natural Science Foundation of China under Grants 61627827, 81630046, 61331001, and 91539127, in part by The National High Technology Research and Development Program of China under Grant 2015AA020901, in part by The Science and Technology Planning Project of Guangdong Province, China under Grants 2015B020233016, 2014A020215031, 2014B020215003, and 2017A020215135, in part by the Young Teachers Scientific Research Cultivating Fund of South China Normal University (16KJ05), and in part by the China Postdoctoral Science Foundation under Grant 2017M610533. Corresponding authors: Zhong Ji and Da Xing (e-mail: jizhong@scnu.edu.cn; xingda@scnu.edu.cn).

Abstract: A near-field transmission-type microwave imaging (NTMI) system was developed to break the bottleneck of the resolution of microwave imaging due to diffraction limitation. The NTMI used a microwave pinhole to control the size of microwave radiation in the near-field region and a high-resolution and highly sensitive detector based on electromagnetic-elastic resonance effect to acquire the transmitted microwave signal. The theoretical analysis and experimental validation showed that the resolution of the NTMI system was up to 1.55 mm, higher than the current resolution ($\sim$cm) of microwave imaging. And the contrast of microwave transmittance based on the different electromagnetic characteristics among various tissues was theoretically deduced and experimentally examined. Moreover, a breast phantom was imaged to estimate the imaging capability of the NTMI system with high contrast (3.7:1–16.7:1) and good tissue penetration ($>$10 cm). Finally, the excised breast of an ewe embedded with an *ex vivo* human breast tumor was imaged clearly with a contrast of about 1:2.8, which is in good agreement with the X-ray image. Therefore, the NTMI system is suitable for noninvasive mass screening and has a great potential for applications in early breast cancer detection.

Index Terms: Near filed, microwave imaging, high resolution and contrast, tumor, electromagnetic characteristics.

1. Introduction

Breast cancer remains as the top threat to women's health, and early diagnosis can significantly improve the survival rate of patients. X-ray mammography remains the golden standard for tumor screening among the screening technologies, it has an inherent limitation such as the ionizing nature of X-rays to limit the mass screening, and it also suffers from a high missed detection and of a procedure that can be uncomfortable, even painful [1]–[3]. The motivation for developing microwave imaging for breast cancer is the significant contrast of normal and malignant breast tissue in their

dielectric properties at microwave frequencies, estimated between 2:1 and 10:1. This indicates that microwave imaging may be useful in detecting tumors that are not visible in X-ray mammography [4]–[7]. Furthermore, the low microwave attenuation in normal breast tissue can achieve good tissue penetration, eliminating the need for uncomfortable or painful breast compression, which may reduce patient compliance with screening recommendations [3]. In particular, microwave radiation has low photon energies (10^{-5}–10^{-2} eV); thus, it is noninvasive radiation and nonthermal damage [8].

However, the challenge of microwave imaging is to break the bottleneck of spatial resolution (∼cm) due to the diffraction limitation, which hinders the development of clinical applications towards early breast cancer detection [9]–[13]. In the recent years, our group have made much effort to improve microwave imaging resolution, and some achievements have been made, mainly in microwave-induced ultrasonic imaging (TAI) based on thermoacoustic effect [14]–[17]. In this paper, we propose a near-field transmission-type microwave imaging (NTMI) method with different principle. The use of a new microwave detector based on electromagnetic-elastic resonance effect (EERE) offers a higher resolution and the sensitivity of a conventional antenna, which has deeply analyzed by our previous work [18]. Most importantly, the size of microwave radiation is controlled by a microwave pinhole in the near-field region. Similar to optical imaging, the resolution of NTMI determined by the size of microwave radiation, which depends on the radius of the pinhole that can be easily set to less than a few millimeters. Therefore, the resolution can achieve orders of subcentimeter (∼mm) and efficiently break the diffraction limitation. NTMI method with the advantages of high resolution and high sensitivity while maintaining the merits of a high contrast, good tissue penetration, and noninvasive radiation of conventional microwave imaging, is potential for clinical applications towards early breast cancer detection.

2. Method and Materials

2.1 Imaging Principle

The contrast of NTMI results from the different microwave signal transmittance of the tissue based on different electromagnetic properties. Here, A simplified model in terms of the basic optical principle involving an optical thin film was discussed. Microwave illuminated the tissue and then interacted with the sample by reflection, absorption, and transmittance. The complex dielectric properties of a tissue can be defined as:

$$\varepsilon_c = \varepsilon - \frac{\sigma}{\omega} j \tag{1}$$

where ε is the dielectric constant and the ability of the materials to be polarized by the external electric field, σ is the conductivity, and ω is the angular frequency of microwave irradiated. The reflection coefficient of microwave on the interface (air /tissue) is:

$$\Gamma = \frac{\eta_c - \eta_o}{\eta_c + \eta_o} \tag{2}$$

in which η_c is the tissue wave impedance [$\eta_c = (\mu/\varepsilon_c)^{1/2}$, μ is the tissue permeability] and $\eta_o = 120\,\pi$ is the spree space wave impedance and a constant.

For a plane wave, the modules of reflection coefficient under the condition $\sigma/\omega\varepsilon << 1$ is given approximately by:

$$|\Gamma| = \frac{\sqrt{\left(\frac{\mu}{\varepsilon} - {\eta_o}^2 - \frac{\mu\sigma^2}{4\varepsilon^3\omega^2}\right)^2 + \frac{\mu\sigma^2}{\varepsilon^3\omega^2}{\eta_o}^2}}{\left(\sqrt{\frac{\mu}{\varepsilon}} + 120\pi\right)^2 + \frac{\mu\sigma^2}{4\varepsilon^3\omega^2}} \tag{3}$$

The reflection coefficient of microwave on the interface (air/tissue) is correlation with their electromagnetic properties. In the NTMI system, the electric field plays a major role than the magnetic field. Therefore, the reflection of microwave is mainly determined by the dielectric properties at the certain radiated microwave frequency. The comparison of dielectric and microwave reflection

TABLE 1
Comparison of the Dielectric Property, Microwave Reflection Coefficient, Absorption Coefficient and Transmittance of Different Biological Sample Tissues at 430 MHz [4], [5].

Sample tissue	Relative permittivity	Conductivity [S/m]	Reflection coefficient	Attenuation coefficient	Transmittance (h = 3 mm)
Fat	5.57	0.04	0.41	3.28	41.6%
Mammary	7.82	0.07	0.48	4.70	34.7%
Glandular	42.3	0.72	0.73	19.77	12.72%
Skin	49.46	0.68	0.75	17.56	11.9%
Muscle	56.90	0.80	0.77	19.33	10.8%
Malignant	67.3	1.02	0.78	22.42	9.4%

properties of different biological tissues such as normal breast, malignant, glandular, fat, muscle, skin and heart at 430 MHz and the calculation results according to (3) were shown in Table 1. The reflection coefficient of the normal breast tissue and fat tissue is about 0.48 and 0.41 respectively, while malignant, muscle, glandular and skin have higher reflection coefficient (0.783, 0.77, 0.73 and 0.75) for the greater dielectric constant and conductivity.

The absorption coefficient in the tissue is written as:

$$\alpha = \omega \sqrt{\frac{\mu\varepsilon}{2}\left[\sqrt{1+\left(\frac{\sigma}{\omega\varepsilon}\right)^2}-1\right]} \tag{4}$$

Previous study has confirmed the significant contrast in the microwave absorption between normal breast tissues and malignant lesion for the dielectric properties [4], [15]. The further study about the microwave absorption properties of different biological tissues (normal breast tissue, fat, malignant, muscle, glandular and skin) and the absorption coefficient calculated by (4) was given in Table 1. It indicated that the adipose dominant tissue such as normal breast tissue and fat tissue interacted with microwave weakly for the lower dielectric constant and conductivity, whereas malignant, muscle, glandular, heart and skin dominated by polar molecules such as water have much greater dielectric constant and conductivity and absorb microwave strongly. Combining (3) and (4), the microwave transmittance of the tissue with thickness of h can be solved. The deducing process was shown in the supplementary material, and the solution is:

$$\begin{aligned} T &= \sum_{i=0}^{n} T_i = \sum_{i=0}^{n} (1-|\Gamma|)\times[(1-h\times\alpha)\times|\Gamma|]^{2n}\times(1-|\Gamma|) \\ &= (1-|\Gamma|)\times(1-h\times\alpha)\times(1-|\Gamma|)\left(1+\frac{[|\Gamma|\times(1-h\times\alpha)]^2}{1-[|\Gamma|\times(1-h\times\alpha)]^2}\right) \end{aligned} \tag{5}$$

According to (5), the microwave transmittance is related to the reflection and absorption of microwave. The higher reflection and absorption of microwave lead to the lower transmittance Therefore, the microwave transmittance of the tissues with thickness of h is also determined by the dielectric properties and approximately in negative correlation with dielectric constant and conductivity at various microwave frequencies. The malignant tissue dominated by polar molecules such as water has a high dielectric constant and conductivity reflects and adsorbs microwave strongly. Thus, the microwave transmittance of malignant tissue (9.4%) and glandular (12.72%) are much lower than normal breast tissue (34.7%) and fat tissue (41.6%) as shown in Table 1. Therefore,

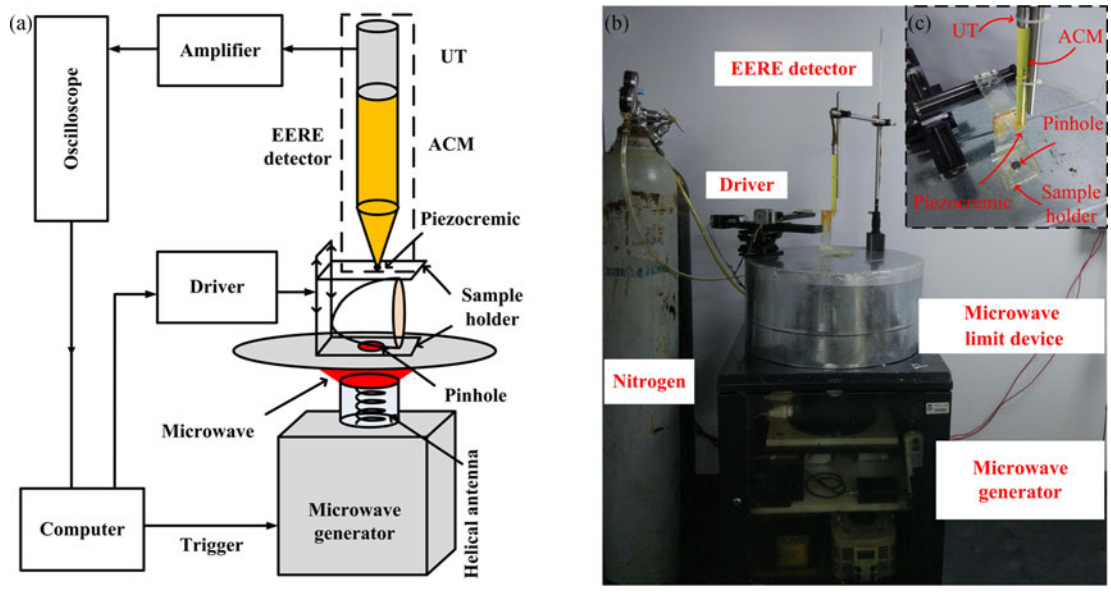

Fig. 1. (a) The schematic diagram of the NTMI breast imaging system. (b) The photograph of the actual setup with close-up view in inset. (c) The detailed photograph of the EERE detector. EERE detector, electromagnetic-elastic resonance effect detector; UT, ultrasound transducer; ACM, acoustic coupling medium.

a new breast screening method based on the differences of microwave transmittance was built, and the contrast is sufficient for the NTMI to differentiate the malignant lesions clearly, particularly in patients with radiographically dense breast tissue, covering the high missed detection rate of X-ray mammography. Besides, most of the biological tissues such as muscle (10.8%) and skin (11.9%) also have different transmittance based on their electromagnetic properties as shown in Table 1, which can potentially be applied for noninvasive evaluation of electromagnetic characteristics among various tissues.

2.2 Imaging System

The schematic diagram of the NTMI system was shown in Fig. 1(a). Microwave beam illuminated the sample after passing through a pinhole, instead of directly radiated by the antenna. And the transmitted microwave signal of the sample was first captured using an EERE transducer and then collected using a computer for data analysis. Considering the tissue penetration and contrast, a 430 MHz microwave generator was used in the following experiments., with the pulse repetition frequencies are typically in the range 1–100 Hz, and the peak output power is tunable from 2 MW to 40 MW with a narrow pulse width (10 ns). The helical antenna with a central frequency of 430 MHz was designed to convert the high-voltage short pulse to microwave radiation. The role of nitrogen is as an insulating gas to prevent conduction in the microwave source. In the near-field region, the energy density around the antenna is adjustable between 18 μJ/cm^2 and 360 μJ/cm^2, which is well within the American National Standards Institute's limits [14]. Besides, the microwave pinhole used to control the size of microwave radiation is made of a metal plate with a pinhole in the middle. The thickness of the metal plate is about 1 mm which enough to shielding microwave except the diffraction of the pinhole, and the size of pinhole is much smaller than the wavelength of microwave and can be changed flexibly. Thus, the microwave spot size is approximately equal to the size of the pinhole due to the limiting effect and the resolution is directly proportional to the size of pinhole, similar to the principle of optical imaging. The high-sensitivity and high-resolution EERE detector instead of a receiving antenna is another critical component of the system, which consists of a piece of piezoceramics with the inherent vibration frequency of 2.5 MHz has a relatively strong EERE,

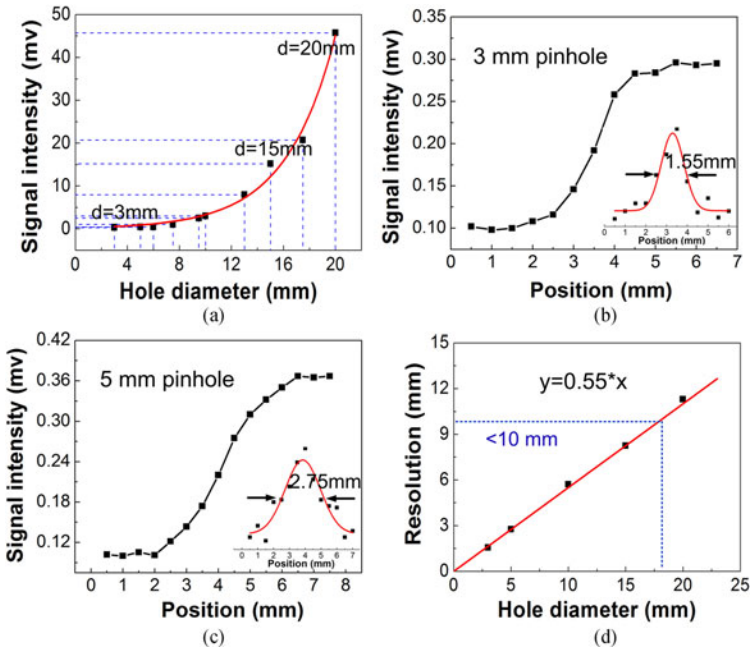

Fig. 2. The near-field diffraction experiment of the pinhole. (a) The influence of different hole diameter on signal. (b) and (c) The resolution with the 3 mm and 5 mm holes respectively. (d) The relationship between hole diameter (x) and resolution (y).

acoustic coupling medium and an ultrasonic receiver (I2.5P10NF, DOPPLER, China) with a central frequency of 2.5 MHz (70% bandwidth at −6 dB). In the course of detection, the antenna, pinhole and EERE detector were fixed in the same axis and the distance of them can be adjusted according to the practical detection as shown in Fig. 1(b). The two-dimensional scanning of NTMI was carried out by a stepper motor to drive the sample holder. The sample holder mainly consists of two piece of thin clear plate with extreme low microwave reflection and absorption properties. The topper can help to hold the sample by moving in the up and down two directions, and the diffraction from the upper is almost negligible. The electrical signal from an ultrasonic receiver was amplified using a custom-made amplifier (0.5–100 MHz, 40 dB), and measured by a commercial oscilloscope (DPO 3034, Tektronix, Ltd.). The signal was finally transferred to a personal computer for subsequent image processing by the direct projection reconstruction algorithm.

3. Results

3.1 SNR and Resolution of the NTMI System

We studied the near-field effects of pinhole and found that the signal-to-noise ratio (SNR) and resolution of the NTMI system depend on the size of the pinhole. The amplitude of microwave signals under different pinhole diameters without sample were detected under the same conditions. That the position of helical antenna and the pinhole is fixed with the distance of about 4 cm, and the EERE detector as far as possible close to the pinhole. The results and fitting curve are shown in Fig. 2(a), and it indicates that the amplitude of microwave signals decreased with decreasing pinhole diameter. When the pinhole diameter was decreased from 20 mm to 3 mm, the microwave signal intensity sharply decreased from 45.7 mV to 0.30 mV. Further research showed that the signal intensity is approximately proportional to the fourth-power exponential function of pinhole diameter, consistent with the subwavelength aperture diffraction theory of small holes reported by Hans Bethe *et al.* in 1942 [19]. Although the pinhole shielded the parts of microwave energy, the weak microwave signal intensity (∼0.3 mV) under 3 mm diameter can still be detected by the high-sensitivity acquisition system of NTMI based on the EERE detector.

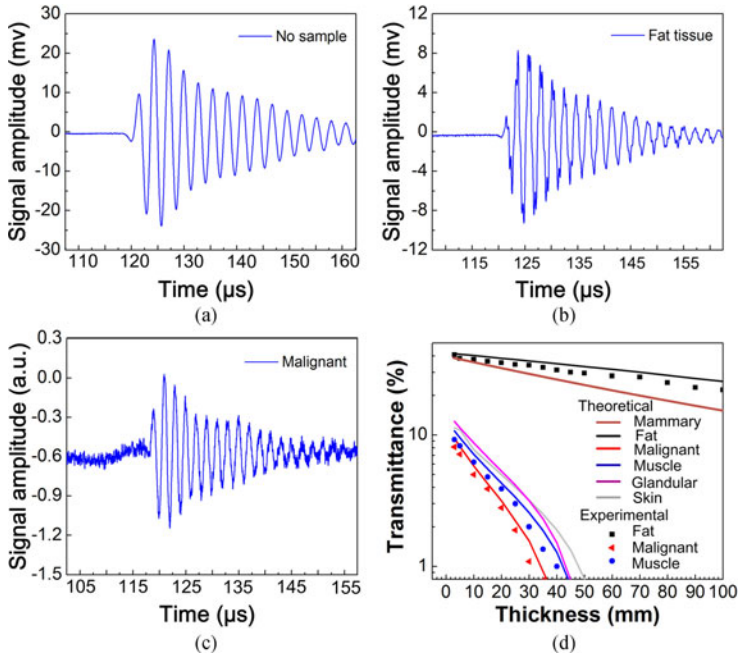

Fig. 3. (a-c) The signal profile of without sample, the fat tissue and the malignant tissue respectively. (d) The comparison of microwave transmittance of different tissues with different thickness.

The relationship between resolution and the size of pinhole is studied by our previous work [18]. In this paper, different sizes of pinholes (3 mm, 5 mm, 10 mm, 15 mm and 20 mm) were comprehensively investigated. A rectangular sheet of an iron sample with the area of more than pinhole was placed on the pinhole, and it was moved at a rate of 0.5 mm/step to detect the signal intensity respectively. The signal intensity decreased to about 0 mV when the pinhole was thoroughly shielded by the sheet of iron. The results of 3 mm and 5 mm pinhole were shown in Fig. 2(b) and (c), and the derivative of the line with Gaussian fitting was inserted in Fig. 2(b) and (c) respectively. The resolution of NTMI system is 1.55 mm and 2.75 mm respectively, as defined by the full-width at half-maximum (FWHM) of the Gaussian fitting [20]. Other pinholes with different sizes of (10 mm, 15 mm and 20 mm) were studied with the same method, and the statistical results showed that the spatial resolution of NTMI was linearly related to the diameter of the pinhole as a function $y = 0.55x$. Thus, a higher resolution ($\sim$mm) can be achieved using a smaller pinhole in theory. When the pinhole was 3 mm, the spatial resolution was up to 1.55 mm under the current experimental conditions. Therefore, a smaller pinhole means a small quantity of microwave radiation will be transmitted, but the system of NTMI still has a potential to make a breakthrough in resolution ($\sim$cm) of conventional microwave imaging. Considering the resolution and SNR, a 15-mm pinhole was used in the phantom study with the subcentimeter resolution ($\sim$8 mm) as shown in Fig. 2. The distance of the pinhole to helical antenna is about 4 cm and the EERE detector to the pinhole is about 12 cm in the following experiment as shown in Fig. 1(b).

3.2 The Contrast of Tissue Transmittance (Malignant and Normal Breast)

The contrast of transmittance based on the different dielectric properties of tissues, further experiments were conducted. The microwave transmittance in NTMI system can be calculated using $T = A_t/A_i$, where A_t is the signal amplitude with the sample, and A_i is the signal amplitude without the sample. The signal profile of no sample was detected by the oscilloscope and given in Fig. 3(a). The signal profiles of fat and malignant which grew on the back of the mouse were provided in Fig. 3(b) and (c) respectively. The transmittance was calculated about 37.64% and 2.52% respectively at the same thickness (20 mm). The further study about the microwave transmittance of

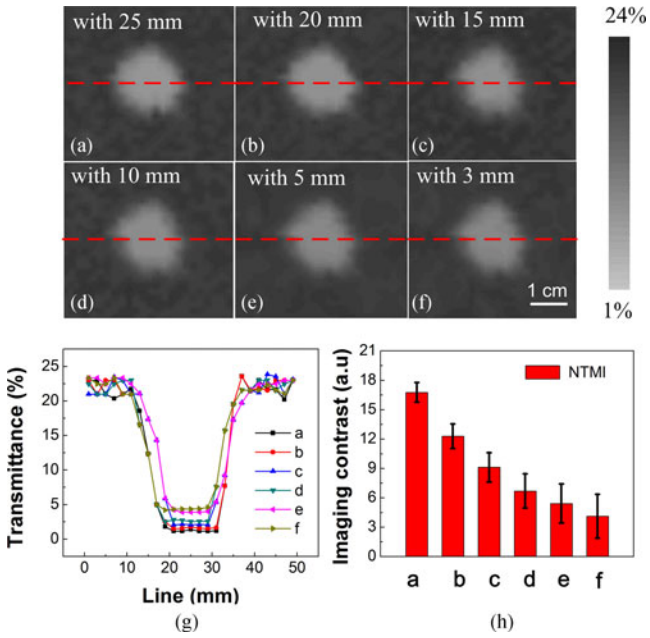

Fig. 4. NTMI of breast phantom. (a-f) The NTMI image of a tumor cut into different thickness of 25 mm, 20 mm, 15 mm, 10 mm, 5 mm and 3 mm respectively and embedded into the phantom. (g) The pixel values of red dotted line shown in (a-f) respectively. (h) The imaging contrast of a tumor with different thickness corresponding to (a-f).

different tissues such as normal breast, malignant, glandular, pork fat, muscle, and skin in theory and experiment was depicted in Fig. 3(d). The experimental results are approximatively consistent with the theory as concluded in (5). It indicated the high contrast of transmittance between malignant and normal breast clearly, and the fat tissue is potential to simulate the normal breast for the similar transmittance in the following phantom experiment. There is a significant contrast between adipose-dominated tissue (normal breast and pork fat tissue) and those tissue (malignant, glandular, muscle and skin) dominated by polar molecules such as water for the much higher dielectric constant and conductivity. And when the normal breast and fat tissue had a thickness of $h = 10$ cm, the microwave transmittance was still about 22.3% and 15.5% respectively. This shows the good depth imaging ability of the NTMI system for breast diagnosis.

3.3 Phantom Experiments

A simple breast phantom was imaged to estimate the imaging capability of the NTMI system. The breast phantom was filled with pork fat tissues which have similar dielectric properties with the normal breast tissues [4]–[7], and the size of the phantom is about 10 cm $\times$ 10 cm $\times$ 10 cm. An excised tumor with size of 21 mm $\times$ 18.4 mm $\times$ 25 mm, which grown on the back of a mouse. In order to put the tumor inserted into the breast, we cut a hole in the breast phantom, remove the corresponding normal tissue, and then fill the hole by the tumor. The NTMI of the breast phantom with the field of view of 5 cm $\times$ 5 cm is shown in Fig. 4(a), and for further demonstration purposes, the excised tumor was cut into different thickness of about 20 mm (b), 15 mm (c), 10 mm (d), 5 mm (e) and 3 mm (f). It can be seen that the microwave transmittance increased with decreasing thickness of tumor. The pixel values of red dotted line in Fig. 4(a)–(f) respectively were given in Fig. 4(g), and it show the microwave transmittance of the sample area of which the malignant lesion is about 1.16%, 1.56%, 2.07%, 2.6%, 3.87% and 4.36% respectively and the simulated normal breast tissue is about 21.27%. Thus, the proposed system of NTMI is potential to image tumor clearly with high contrast (3.7:1–16.7:1) at 10 cm thickness as shown in Fig. 4(h).

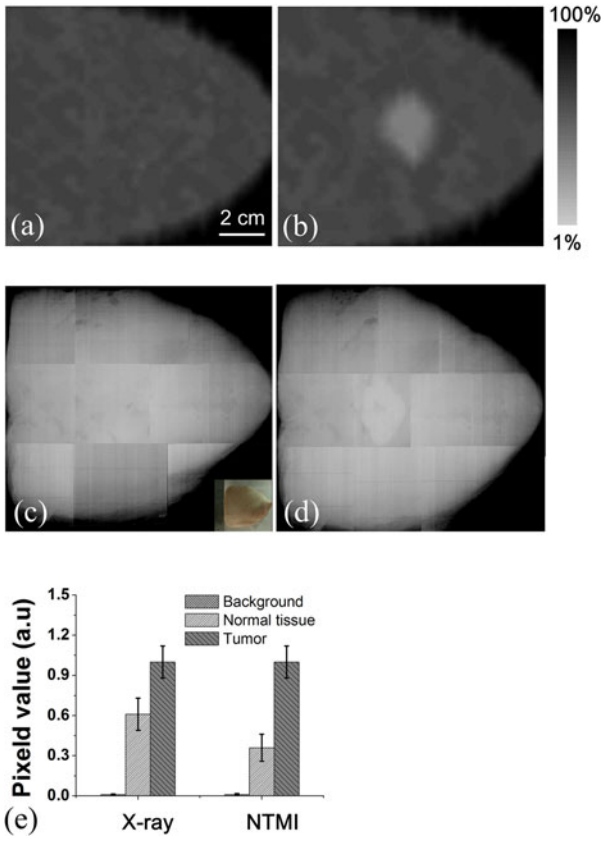

Fig. 5. NTMI of the excised breast of ewe. (a) and (b) The breast of ewe without and with an excised breast tumor. (c) and (d) X-ray images responding to (a) and (b). (e) The normalized image contrast between tumor, normal tissue and background.

3.4 Breast of Ewe Experiment

To further demonstrate the imaging capability of the NTMI system, a breast phantom was built, which mainly composed of excised human breast tumor and the excised breast of an adult ewe. All of the experiments involved animal and human tissues in this paper have passed a protocol approved by the Institutional Review Board of the South China Normal University (Project number: 81630046). The excised breast of an adult ewe with the diameter of about 12 cm. The excised human breast tumor was obtained from the Sun Yat-Sen University Cancer Hospital, and its size is about 31.7 mm $\times$ 23.6 mm $\times$ 11.8 mm. The NTMI results of the normal breast and the tumor embedded breast were shown in Fig. 5(a) and (b), respectively. The corresponding X-ray image which spliced from ten X-ray pictures due to the restricted field of view of our x-ray machine, was shown in Fig. 5(c) and (d). It can be observed that the shape is accurately matched with the NTMI. To explore the imaging contrast, the normalized pixel values of the normal tissue, tumor, and the background in the NTMI and X-ray ware shown statistically in Fig. 5(e), all error bars represent three times experimental statistical results. The difference between the normal tissue and the tumor can be clearly seen in the NTMI with a mean contrast of about 1:2.8, while it has a mean contrast of about 1:1.8 in the X-ray. The X-ray mammography is based on the transmittance of X-ray for the difference of density. NTMI is a kind of parallel to the X-ray imaging mode, which based on the microwave transmittance due to the different dielectric properties, with a higher contrast. More importantly, the noninvasive radiation is suitable for mass screening and the good depth imaging ability ($h > 10$ cm) of NTMI is potential to eliminate the need for uncomfortable or painful breast compression in breast cancer detection. This would allow more comfortable screening recommendations.

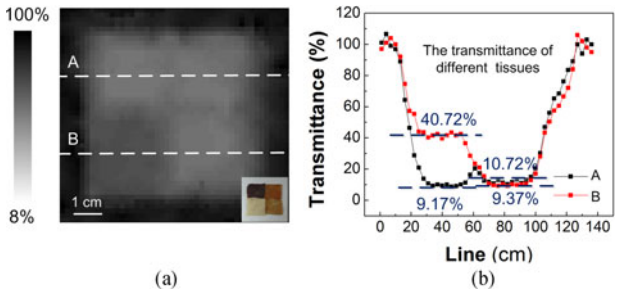

Fig. 6. (a) The phantom imaging of different biological tissues (heart, lung, fat and muscle). (b) The pixel values of line A, B in (a).

4. Discussion and Conclusion

A great improvement in spatial resolution was achieved, thus breaking the bottleneck of the resolution of microwave imaging by diffraction limitation. In this paper, the theoretical analysis and experimental validation confirmed that NTMI has the advantages of high resolution, high contrast, good tissue penetration, and noninvasive radiation. Thus, NTMI has the great possibility to become an alternative or supplement to the widely-used X-ray mammography for early breast cancer detection. One the other hand, NTMI reflects the dielectric properties of the tissues based on the different transmittance which have been theoretically studied in Table 1 and experimentally verified in Fig. 3(d). This wide range of transmittance among various tissues can potentially be applied for noninvasive evaluation of electromagnetic characteristics. As a demonstration, the phantom imaging of different biological tissues (heart, lung, fat, and muscle) was carried out, and the results are shown in Fig. 6(a). The sizes of the individual heart, lung, fat, and muscle tissue are about 3.5 cm $\times$ 3.5 cm $\times$ 3.3 mm, as shown in Fig. 6(a). Furthermore, the mean pixel values of lines A and B in Fig. 6(a) are shown in Fig. 6(b); the microwave transmittance of the sample area of fat ($\sim$40.72%) is higher than that of muscle ($\sim$9.37%), heart ($\sim$9.17%), and lung ($\sim$10.72%) tissues for different dielectric properties. Therefore, NTMI reflecting the dielectric property of the tissue can be obtained by reconstructing the distribution of microwave transmittance T. Thus, it has a great potential for the noninvasive evaluation of electromagnetic characteristics towards biological tissues.

In the NTMI system, the sample was moved step by step in a two-dimensional scanning platform, and the signal intensity of each step was gathered in the computer, in which a microwave image was reconstructed. So the time to form one image is:

$$t = t_1 + t_2 = \frac{a}{f} \times N + t_3 \times N$$

Where t_1, t_2 is total time of signal acquisition and motor movement respectively, a is the number of average of per step, f is the microwave repetition frequency, N is the number of pixels, t_3 is the time of motor movement of per step. For example, in Fig. 4, the phantom with the size of 10 cm $\times$ 10 cm $\times$ 10 cm was moved at a rate of 2.5 mm/step ($t_3 = 20$ ms/step) to detect the signal intensity respectively with the mean times $a = 10$, the microwave repeat frequency of 100 Hz, and the number of pixels $N = (100\,\text{mm} \times 100\,\text{mm})/2.5\,\text{mm/step} = 1600$, so under the microwave repetition frequency of 100 Hz the time to form the image is:

$$t = t_1 + t_2 = \frac{10}{100} \times 1600 + 0.02 \times 1600 = 192s.$$

In the current system, the mechanical scanning is indeed some slow in contrast to X-ray. In order to improve the measurement speed, one way is that increasing the signal-to-noise ratio can reduce the average number of times to shorten the acquisition time. Another way is the using of high-speed motor to shorten the motor moving time. Since the principle of NTMI system is similar as that of X-ray, the imaging speed has the possibility to approach X-ray in future.

The traditional microwave imaging can measure the depth of abnormalities, but in our system, only amplitude of transmission is seen, which is caused by projection. A possible way to solve this problem is that, after finding a suspicious area, repeat the imaging process in the vertical direction, then the depth information can be extracted. This way is simple and easy to operation, but double the imaging time.

The microwave transmittance theory in this study considered a simple plane wave normal incidence. However, the actual waveforms may be more diverse, not just plane waves, but also spherical waves. In addition to the actual incident, there may be oblique incidence or both normal incidence and oblique incidence, even more complex situations, which need further investigation. The polarization direction may need to take account linear polarization, elliptical polarization, and circular polarization. In fact, the shapes of the targets may be diverse, and the electrical parameters change over time due to various reasons [5]. Therefore, a more accurate model of the microwave transmittance theory will be considered in the next step. On the other hand, a microwave anti-reflection coating on the pinhole between air and sample medium may significantly improve the energy efficiency and achieve a better image quality of NTMI by reducing the amounts of microwave reflection.

Reference

[1] P. T. Huynh, A. M. Jarolimek, and S. Daye, "The false-negative mammogram," *Radiographics*, vol. 18, no. 5, pp. 1137–1154, 1998.

[2] V. P. Jackson, R. E. Hendrick, S. A. Feig, and D. B. Kopans, "Imaging of the radiographically dense breast," *Radiology*, vol. 188, no. 2, pp. 297–301, 1993.

[3] S. H. Heywang-Kobrunner, "Nonmammographic breast imaging techniques," *Curr. Opin. Radiol.*, vol. 4, no. 5, pp. 146–154, 1992.

[4] W. T. Joines, Y. Zhang, C. Li, and R. L. Jirtle, "The measured electrical properties of normal and malignant human tissues from 50 to 900 MHz," *Med. Phys.*, vol. 21, pp. 547–550, 1994.

[5] T. Sugitani *et al.*, "Complex permittivities of breast tumor tissues obtained from cancer surgeries," *Appl. Phys. Lett.*, vol. 104, no. 25, 2014, Art. no. 253702.

[6] X. Li and S. C. Hagness, "A confocal microwave imaging algorithm for breast cancer detection," *IEEE Microw. Wireless Compon. Lett.*, vol. 11, no. 3, pp. 130–132, Mar. 2001.

[7] L. Nie, D. Xing, and S. Yang, "In vivo detection and imaging of low-density foreign body with microwave-induced thermoacoustic tomography," *Med. Phys.*, vol. 36, no. 8, pp. 3429–3437, 2009.

[8] Z. Ji, C. Lou, Y. Shi, W. Ding, S. Yang, and D. Xing, "A microwave detection way by electromagnetic and elastic resonance: Breaking the bottleneck of spatial resolution in microwave imaging," *Appl. Phys. Lett.*, vol. 107, no. 16, 2015, Art. no. 164103.

[9] N. Nikolova, "Microwave imaging for breast cancer," *IEEE Microw. Mag.*, vol. 7, no. 12, pp. 78–94, Dec. 2011.

[10] E. C. Fear, "Microwave imaging of the breast," *Technol. Cancer. Res. Treatment*, vol. 4, no. 1, pp. 69–82, 2005.

[11] W. C. Khor, M. E. Bialkowski, A. Abbosh, N. Seman, and S. Crozier, "An ultra wideband microwave imaging system for breast cancer detection," *IEICE Trans. Commun.*, vol. 90, no. 9, pp. 2376–2381, 2007.

[12] F. C. Chen and W. C. Chew, "Experimental verification of super resolution in nonlinear inverse scattering," *Appl. Phys. Lett.*, vol. 72, no. 23, pp. 3080–3082, 1998.

[13] S. Y. Semenov *et al.*, "Microwave-tomographic imaging of the high dielectric-contrast objects using different image-reconstruction approaches," *IEEE Trans. Microw. Theory Techn.*, vol. 53, no. 7, pp. 2284–2294, Jul. 2005.

[14] C. Lou, S. Yang, Z. Ji, Q. Chen, and D. Xing, "Ultrashort microwave-induced thermoacoustic imaging: A breakthrough in excitation efficiency and spatial resolution," *Phys. Rev. Lett.*, vol. 109, no. 21, 2012, Art. no. 218101.

[15] F. Ye, Z. Ji, W. Ding, C. Lou, S. Yang, and D. Xing, "Ultrashort microwave-pumped real-time thermoacoustic breast tumor imaging system," *IEEE Trans. Med. Imag.*, vol. 35, pp. 839–844, Mar. 2016.

[16] C. Zhang and Y. Wang, "A reconstruction algorithm for thermoacoustic tomography with compensation for acoustic speed heterogeneity," *Phys. Med. Biol.*, vol. 53, no. 18, pp. 4971–4982, 2008.

[17] Y. Xu and L. V. Wang, "Effects of acoustic heterogeneity in breast thermoacoustic tomography," *IEEE. Trans. Ultrason. Ferroelect. Freq. Control*, vol. 50, no. 9, pp. 1134–1146, Sep. 2003.

[18] Z. Ji, C. Lou, Y. Shi, W. Ding, S. Yang, and D. Xing, "A microwave detection way by electromagnetic and elastic resonance: Breaking the bottleneck of spatial resolution in microwave imaging," *Appl. Phys. Lett.*, vol. 107, no. 16, 2015, Art. no. 164103.

[19] F. Gao, Y. Zheng, and D. Wang, "Microwave-acoustic phasoscopy for tissue characterization," *Appl. Phys. Lett.*, vol. 101, no. 4, 2012, Art. no. 043702.

[20] F. Gao, Q. Zheng, and Y. Zheng, "Electrical circuit modeling and analysis of microwave acoustic interaction with biological tissues," *Med. Phys.*, vol. 41, no. 5, 2014, Art. no. 053302.

[21] H. A. Bethe, "Theory of diffraction by small holes," *Phys. Rev.*, vol. 66, nos. 7/8, pp. 163–182, 1944.

[22] Z. Chen, S. Yang, Y. Wang, and D. Xing, "All-optically integrated photo-acoustic microscopy and optical coherence tomography based on a single Michelson detector," *Opt. Lett.*, vol. 40, no. 12, pp. 2838–2841, 2015.